RESEARCH PAPER | Physics | Volume : 5 | Issue : 8 | August 2015 | ISSN - 2249-555X

Structural and Non-linear optical behavior analysis of 1-(3-methoxyphenyl)-5-Phenyl-2, 4-Pentadiene-3-one using DFT calculations

KEYWORDS: FT-IR and FT- Raman; DFT; Vibrational analysis; HOMO-LUMO;

D. Sumathi	H. Saleem	S. Srinivasan
Department of Physics, Annamalai University, Annamalainagar-608002, Tamil nadu, India.	Department of Physics, Annamalai University, Annamalainagar-608002, Tamil nadu, India.	Department of Chemistry (DDE Wing), Annamalai University, Annamalainagar-608002, Tamil nadu, India.

S. Manivarman	S. Subashchandrabose	A.Dhandapani
PG & Research Department of Chemistry, Government Arts College, Chidambaram -608102, Tamil nadu, India.	Centre for Research and development, PRIST University, Thanjavur – 613 403, Tamil nadu, India.	PG & Research Department of Chemistry, Government Arts College, Chidambaram -608102, Tamil nadu, India.

ABSTRACT *Chalcone derivative of 1-(3-methoxyphenyl)-5-Phenyl-2,4-Pentadiene-3-one was synthesized. To characterize the molecular structure and its functional groups the Fourier-Transform infrared (FTIR) and Fourier-Transform Raman (FT-Raman) spectra of (MPPDO) was recorded in the region 4000–400 cm-1 and 3500–50 cm-1. Quantum chemical calculation of energies, geometrical structure and vibrational wavenumber of MPPDO were carried out by DFT/B3LYP/6-311++G(d,p) level of theory. The vibrational frequencies are calculated at DFT level and compared with FT-IR and FT-Raman experimental values. The difference between the observed and scaled wavenumber values of most of the fundamentals is very small. The optical behavior through first order hyperpolarizability, intra-molecular charge transfer and energy difference between valence band and conduction band gap were calculated using B3LYP/6-311++G(d,p) basis set. The electronic transition was studied using UV-Vis spectrum and the observed value were compared with the theoretical value. The MEP surface of the title molecule was also analyzed using the same level of basis set.*

1. Introduction

Chalcones are highly reactive substances of varied nature and can be used as an initial compound for synthesis of various compounds. It possess many interesting pharmacological activities [1] like anti-inflammatory, antimicrobial, antifungal, antioxidant, cytotoxic, antitumor and anticancer activities [2, 3]. Chalcones are also finding application as organic nonlinear optical materials (NLO) for their SHG conversion efficiency [4]. The basic skeleton of chalcones which possess α, β-unsaturated carbonyl group is useful for the synthesis of various biodynamic cyclic derivatives such as pyrazoline, benzodiazepine, 2,4,6-triaryl pyridine, isoxazoline and cyclohexenone [5, 6, 7, 8, 9, 10]. In the present study, the title molecule (MPPDO) was synthesized and the spectral characterizations were made by FT-IR, FT-Raman and UV-Visible spectra and the corresponding theoretical predictions were carried out using B3LYP/6-311++G(d, p) level of calculations.

2. Experimental details

2.1 Synthesis

A solution of 3-methoxy benzaldehyde (1g) and monobenzal acetone (1g) in aqueous ethanol (70%) containing sodium hydroxide (1g) was heated over a water bath and refluxed for 6 hours. The solution gradually turned yellow crystals, reflux was stopped and solution cooled. The product was filtered, washed with cold water until the washings were neutral to litmus and then washed with 20 ml of ice-cold rectified spirit. The crude title compound was dried in air, it was weighed 0.561g. Then it was recrystallized from rectified spirit, the yield of pure compound a pale yellow solid was 0.301g.

2.2 FT-IR, FT-Raman and UV–Vis., spectra

The FT-IR spectrum of MPPDO was recorded in the spectral region between 400–4000 cm^{-1} using the KBr pellet technique. The spectrum was recorded at room temperature with a scanning speed of 10 cm^{-1} per minute and at the spectral resolution of 2.0 cm^{-1} in the Department of Chemistry, Annamalai University, Annamalai Nagar Tamilnadu, and India. The FT-Raman spectrum of title compound was recorded using the 1064 nm line of an Nd:YAG laser as excitation wavelength in the region 50–3500 cm^{-1} on Bruker model IFS 66V Spectrophotometer equipped with an FRA 106 FT-Raman module accessory and at spectral resolution of 4 cm^{-1}. The FT-Raman spectral measurement was carried out from SAIF Laboratory, IIT Madras, and Tamilnadu, India. The ultraviolet (UV) absorption spectrum of MPPDO was recorded in the range of 200–500 nm using a Shimadzu – 2600 Spectrometer, UV pattern is taken from a 10^{-5} molar solution of MPPDO dissolved in benzene.

3. Computational Details

For meeting the requirements of both accuracy and computing economy, theoretical methods and basis sets should be considered. DFT has proved to be extremely useful in treating electronic structure of molecules. The density functional three parameter hybrid model (DFT/B3LYP/6-311++G(d,p) basis set was adopted to calculate the properties of the title molecule in this work. All the calculations were performed using the Gaussian 03W program package [11] with the default convergence criteria without any constraint on the geometry [12]. It should be noted that Gaussian 03W package does not calculate the Raman intensities. The Raman activities were transformed into Raman

Volume : 5 | Issue : 8 | August 2015 | ISSN - 2249-555X

intensities using Raint program [13] by the expression:

$$I_i = 10^{-12} \times (\upsilon_o - \upsilon_i)^4 \times 1/\upsilon_i \times RA_i \quad (1)$$

Where I_i is the Raman intensity, RA_i is the Raman scattering activities, υ_i is the wavenumber of the normal modes and υ_o denotes the wavenumber of the excitation laser [14]. For B3LYP functional, selected as the one which gives the most accurate results, calculations were continued with the expanded 6-311++G(d,p) basis set. The results obtained at this level of theory, were used for the detailed interpretation of the IR and Raman spectra. TED was calculated by using the VEDA4 program [15, 16] and the fundamental vibrational modes were characterized by their TED.

4. Result and Discussion

4.1 Molecular Geometry

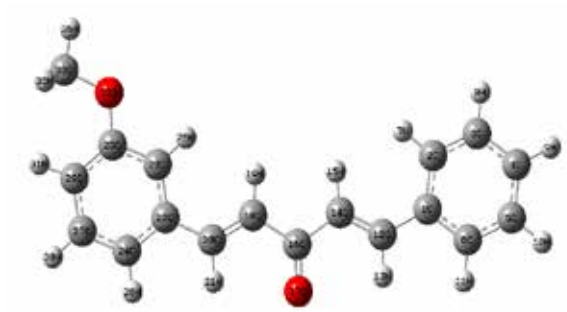

The most stable conformer of the title compound belongs to C_1 point group symmetry. The optimized molecular structure of MPPDO is shown in Figure. 1. The Optimized bond lengths, bond angles and dihedral angles of the molecule are calculated using B3LYP/6-311++G(d,p) level and are listed in Table 1.

Figure.1 Optimized structure of (1E,4E)-1- (3-methoxyphenyl) -5-phenylpenta-1,4-dien-3-one.

Our title compound, consist of carbonyl and methoxy functional groups and plays an major influence in its activity. A carbon-oxygen bond is one of the most abundant in organic chemistry and biochemistry. In this study, the bond distance of C_{16}=O_{17} is 1.227 Å. Samshuddin et al., [17] and Sudha et al., [18] reported the C=O bond lengths are 1.229 Å and 1.190 Å in the case of (1E,4E)-1-(3-Nitrophenyl)-5-phenylpenta-1,4-dien-3-one and 1,5-diphenyl penta-1-4 dien-3-one respectively which shows that, the calculated value is in agreement with above literature value. It is observed that, the average C-C bond length in MPPDO for both phenyl rings is ~1.397 Å, while the literature value is about 1.4 Å [19]. Similarly the calculated C-H bond lengths of phenyl rings are also in agreement with literature [19]. In MPPDO, the average C-C-C bond angle in both phenyl rings is found to be ~120° which represent the symmetry of the benzene rings. The shorting of the bond angle (O_{32}-C_{33}-H_{36}: 105.78°) in methyl group may be due to the electro negativity of O_{32} atom. The optimized structure is planar as it is evident from the dihedral angles C_{18}–C_{20}–C_{22}–C_{23}= −0.00° or C_{18}–C_{20}–C_{22}–C_{24}= −179.99° and C_6–C_1–C_{12}–C_{14}= −180.00° or C_2–C_1–C_{12}–C_{14}= −0.00° are shown in Table 1. Although the differences, calculated geometrical parameters represent a good approximation and they can be used as foundation to calculate the other parameters, such as vibrational frequencies and thermodynamics properties.

Table.1 The optimized Bond parameters of MPPDO using B3LYP/6-311++G (d,p) level.

BondLengths (Å)	DFT	BondAngles (°)	DFT
C1-C2	1.407	C2-C1-C6	118.08
C1-C6	1.405	C2-C1-C12	123.32
C1-C12	1.462	C6-C1-C12	118.58
C2-C3	1.388	C1-C2-C3	120.80
C2-H7	1.084	C2-C3-C4	120.33
C3-C4	1.397	C3-C4-C5	119.66
C3-H8	1.084	C4-C5-C6	119.97
C4-C5	1.393	C1-C6-C5	121.14
C4-H9	1.084	C1-C12-C14	128.06
C5-C6	1.392	C12-C14-C16	121.11
C5-H10	1.084	C14-C16-O17	122.13
C6-H11	1.085	C14-C16-C18	115.68
C12-H13	1.088	O17-C16-C18	122.18
C12-C14	1.345	C16-C18-C20	121.12
C14-H15	1.085	C18-C20-C22	128.07
C14-C16	1.485	C20-C22-C23	122.91
C16-O17	1.227	C20-C22-C24	118.41
C16-C18	1.484	C23-C22-C24	118.66
C18-H19	1.085	C22-C23-C25	120.87
C18-C20	1.345	C22-C24-C27	120.29
C20-H21	1.088	C23-C25-C29	120.06
C20-C22	1.463	C23-C25-O32	115.61
C22-C23	1.399	C29-C25-O32	124.32
C22-C24	1.408	C24-C27-C29	120.90
C23-C25	1.395	C25-C29-C27	119.18
C23-H26	1.083	C25-O32-C33	118.71
C24-C27	1.388	O32-C33-H36	105.78
C24-H28	1.084	Dihedral Angles (°)	
C25-C29	1.400	C6-C1-C2-C3	-0.00
C25-O32	1.365	C6-C1-C2-H7	-180.00
C27-C29	1.396	C12-C1-C2-C3	179.99
C27-H30	1.084	C2-C1-C12-C14	-0.00
C29-H31	1.082	C6-C1-C12-H13	-0.00
O32-C33	1.422	C6-C1-C12-C14	-180.00
C33-H34	1.095	C18-C20-C22-C23	0.00
C33-H35	1.095	C18-C20-C22-C24	-179.99
C33-H36	1.089	H21-C20-C22-C23	-179.99

4.2 Vibrational Assignments

The title compound consist of 36 atoms and has C_1 point group of symmetry. Hence 102 normal modes of vibrations are possible. These normal modes of MPPDO distributed with 69 in-plane vibrations and 33 out-of-plane vibrations. All the vibrations are active in both Raman and IR absorption. A detailed vibrational description given by means of normal mode analysis and compared theoretically scaled wavenumber with PED. In order to obtain the spectroscopic analysis of the selected compound, the PED analysis has been carried out for MPPDO using VEDA4 program [20] and presented in Table 2. Furthermore, the none of the predicted vibrational spectra have any imaginary frequency, implying that the optimized geometry is located at the local lowest point on the potential energy surface. The DFT potentials systematically overestimate the vibrational wavenumbers. These discrepancies are corrected by computing anharmonic corrections explicitly or by introducing a scaled field or directly scaling the calcu-

Volume : 5 | Issue : 8 | August 2015 | ISSN - 2249-555X

lated wavenumbers with the proper factor [21]. Considering systematic error, we have adopted the scaling factor of 0.9608 for B3LYP method. The observed and calculated vibrational wavenumbers using DFT(B3LYP/6-311++G(d,p) along with their relative intensities and Raman scattering activities are given in Table 2. To understand the spectral features, a comparison of stimulated and observed FT-IR and FT-Raman spectra of MPPDO are presented in Figure 2 and Figure 3, respectively. The observed and calculated wavenumbers are tabulated in Table 2.

4.2.1 O–CH_3 Vibrations

The wavenumbers of the vibrational modes of methoxy groups in MPPDO are known to be influenced by a variety of interesting interactions such as electronic effects, intermolecular hydrogen bonding in the crystalline network [22] and Fermi resonance. Electronic effects such as back-donation and induction, mainly caused by the presence of oxygen atom adjacent to CH3 group, can shift the position of C–H stretching and bending modes [23–25]. Meganathan et al., [26] observed C–H stretching vibrations of methoxy group bands at 2977, 2828, 2838 cm−1 in FT-IR (solid phase). Poiyamozhi et al., [27] observed C-H stretching vibrations in methoxy group bands at 3019 and 2947 cm−1 in FT-IR. In accordance with this in the present study, the C–H stretching vibrations in methoxy group observed at 2834, 2917 cm−1 in FT-IR spectrum and their corresponding FT-Raman values 2836, 2911 cm−1 are assigned to C–H symmetric and asymmetric stretching vibrations, respectively. The TED corresponding to these vibrations contributes more than 90%. For the same mode the theoretically scaled values (mode nos. 16, 17) 2888 and 2945 cm−1 are in moderate agreement with the experimental values. The mode: 26 (1446 cm-1) assigned to CH3 scissoring vibration which is in agreement with the literature value (1455 cm-1) [26]. The very strong band at 1129 cm-1 in FTIR assigned to CH3 twisting mode [26], where as the harmonic band at 1121/mode no:46 is assigned to the same mode. The νO–CH3 vibration mode is assigned at ~1040 cm−1 for anisole [28] and in the region of 1000–1100 cm−1 for anisole and its derivatives [29–32]. This mode is assigned at 1026, 909 and 995 cm−1 for *o*-, *m*- and *p*-methoxybenzaldehydes, respectively. In this study, the O–CH3 stretching mode is assigned to a strong FT-IR band at 1042(w) cm−1 while the Raman counterpart is at 1030(vw). For the same mode the calculated value 1032 cm-1/ mode no: 50 is in good agreement with experimental values. Singh and Yadav [33] assigned the C–O–CH3 angle bending mode at 341, 382 and 430 cm−1 for the o-, m- and p-methoxybenzaldehydes, respectively. Based on the above literature the mode no: 85/393 cm-1 assigned to βCOCH3 mode. Lakshmaiah and Ramanarao [30] assigned the CH3 torsion mode to be at 58 cm-1 for anisole. In MPPDO the mode no: 99 (57 cm-1) is attributed to the same mode.

Table.2 The experimental and calculated frequencies of MPPDO.

S. No.	Calculated values		Observed values		Intensities		Vibrational Assignments≥10% (TED)[c]
	Un scaled	scaled	FT-IR	FT-Raman	IR	Raman	
1	3208	3082			0.85	0.29	$\nu C_{29}H_{31}$(91)
2	3197	3072			0.3	0.06	$\nu C_{23}H_{26}$(98)
3	3193	3068			2.05	0.56	νC_2H_7(93)
4	3186	3061		3060w	3.13	0.13	νC_3H_8(84)+νC_6H_{11}(11)
5	3186	3061			1.61	0.23	$\nu C_{18}H_{19}$(60)+$\nu C_{27}H_{30}$(33)
6	3178	3053			0.8	0.23	νC_2H_7(69)+νC_6H_{11}(16)
7	3170	3046			0.44	0.17	$\nu C_{18}H_{19}$(28)+$\nu C_{27}H_{30}$(46)
8	3170	3046			0.79	0.05	νC_2H_7(12)+νC_6H_{11}(35)+$\nu C_{27}H_{30}$(13)
9	3167	3043			0.98	0.15	νC_3H_8(16)+$\nu C_{12}H_{13}$(36)+$\nu C_{18}H_{19}$(36)
10	3163	3039			0.37	0.02	νC_4H_9(73)+νC_6H_{11}(20)
11	3158	3035			0.33	0	$\nu C_{14}H_{15}$(47)+$\nu C_{23}H_{26}$(43)
12	3148	3024	3026vw		0.06	0.07	$\nu C_{20}H_{21}$(93)
13	3144	3021			0.07	0.05	$\nu C_{12}H_{13}$(94)
14	3135	3012			2.3	0.21	$\nu C_{33}H_{36}$(91) (asy)

Volume : 5 | Issue : 8 | August 2015 | ISSN - 2249-555X

15	3065	2945	2917vw	2911vw	4.15	0.14	$\nu C_{33}H_{35}(98)$ (asy)
16	3005	2888	2834w	2836vw	7.37	0.37	$\nu C_{33}H_{34}(92)$ (sym)
17	1727	1659	1654w		6.65	6.49	$\nu O_{17}C_{16}(51)+\nu C_{12}C_{14}(19)$
18	1663	1598	1601m	1598vs	100	1.68	$\nu C_{12}C_{14}(18)+\nu C_{18}C_{20}(37)+\beta H_{11}C_6C_1(11)$
19	1645	1581			9.06	1.32	$\nu C_{23}C_{22}(51)$
20	1639	1575			3.27	2.78	$\nu C_{12}C_{14}(21)+\nu C_{23}C_{22}(10)+\nu C_1C_2(11)+\beta H_7C_2C_1(11)$
21	1623	1560			11.86	100	$\nu O_{17}C_{16}(28)+\nu C_5C_4(22)+\nu C_1C_6(10)$
22	1612	1549			7.44	11.43	$\nu C_{18}C_{20}(11)+\nu C_6C_5(33)$
23	1611	1547			4.14	2.38	$\nu C_{23}C_{22}(12)+\nu C_{22}C_{24}(35)+\beta H_{31}C_{29}C_{27}(12)$
24	1526	1466	1489w		1.57	0.95	$\beta H_7C_2C_1(44)+\beta H_{11}C_6C_1(15)$
25	1515	1455	1451w	1450vw	8.75	0.06	$\nu C_{22}C_{23}(12)+\nu C_{22}C_{24}(13)+\beta H_{26}C_{23}C_{25}(46)$
26	1505	1446			1.04	0.12	$\beta H_{34}C_{33}H_{35}(70)+\beta H_{35}C_{33}H_{36}(15)$
27	1492	1434	1432vw		1.04	0.15	$\beta H_{34}C_{33}O_{32}(11)+\tau H_{34}C_{33}O_{32}C_{25}(82)$
28	1482	1424			6.31	2.03	$\nu C_{23}C_{22}(11)+\beta H_{35}C_{33}H_{36}(39)$
29	1479	1421			3.4	0.67	$\nu C_1C_6(18)+\beta H_7C_2C_1(51)$
30	1467	1410			9.82	0.21	$\nu C_{22}C_{23}(13)+\beta H_{31}C_{29}C_{27}(15)+\beta H_{34}C_{33}H_{35}(14)+\beta H_{35}C_{33}H_{36}(25)$
31	1365	1311	1319vw	1312vvw	21.29	1.16	$\beta H_7C_2C_1(10)+\beta H_8C_3C_4(17)+\beta H_{11}C_6C_1(27)$
32	1359	1306			9.43	1.36	$\nu C_3C_2(13)+\beta H_7C_2C_1(10)+\beta H_{11}C_6C_1(11)+\beta H_{19}C_{18}C_{20}(11)$
33	1356	1303			2.59	0.4	$\nu C_{22}C_{23}(51)+\nu C_{22}C_{24}(13)+\beta H_{26}C_{23}C_{22}(13)$
34	1352	1299			0.11	4.18	$\nu C_3C_2(22)+\nu C_3C_2$ (11)$+\beta H_{11}C_6C_1(14)+\beta H_{19}C_{18}C_{20}(17)$
35	1338	1286			0.21	0.49	$\nu C_1C_6(12)+\beta H_{21}C_{20}C_{18}(31)$
36	1330	1278		1275vw	3.04	0.12	$\beta H_{13}C_{12}C_{14}(38)+\beta H_{19}C_{18}C_{20}(16)$
37	1314	1263	1259w		10.62	1.73	$\nu O_{32}C_{25}(15)+\beta H_{26}C_{23}C_{22}(21)+\beta H_{31}C_{29}C_{27}(14)$
38	1301	1250			7	6.23	$\nu C_1C_2(12)+\nu C_1C_{12}(18)+\beta H_{11}C_6C_1(20)$
39	1254	1204			21.19	0.81	$\nu O_{32}C_{25}(16)+\beta H_{19}C_{18}C_{20}(25)+\beta H_{26}C_{23}C_{25}(20)$
40	1228	1180		1182w	1.7	3.42	$\nu C1C6(14)+\nu C20C22(16)+\beta H7C2C1(12)+\beta H15C14C16(18)$
41	1215	1167			1	3.15	$\beta H_{30}C_{27}C_{29}(15)+\Gamma C_{35}H_{33}O_{32}H_{25}(35)$

Volume : 5 | Issue : 8 | August 2015 | ISSN - 2249-555X

42	1203	1156	1156w		2.25	4.08	$\beta H_7C_2C_1(30)+\beta H_8C_3C_4(12)+\beta H_{11}C_6C_1(30)$
43	1196	1149			0.35	0.26	$\nu C_{24}C_{27}(15)+\beta H_{28}C_{24}C_{27}(45)+\Gamma C_{35}H_{33}O_{32}H_{25}(20)$
44	1184	1137			0.15	0.26	$\beta H_{15}C_{14}C_{16}(75)$
45	1178	1132			8.03	1.84	$\nu C_{29}C_{25}(12)+\nu O_{32}C_{25}(10)+\nu O_{32}C_{33}(15)+\beta H_{28}C_{24}C_{27}(10)+\Gamma C_{35}H_{33}O_{32}H_{25}(10)$
46	1166	1121			0.08	0.04	$\beta H_{34}C_{33}O_{32}(75)+\Gamma H_{34}C_{33}O_{32}C_{25}(20)$
47	1117	1073	1096vw	1081vvw	8.23	0.03	$\nu C_{27}C_{29}(45)+\beta H_{31}C_{29}C_{27}(15)$
48	1107	1063			22.63	0.34	$\nu C_1C_6(22)+\nu C_{14}C_{16}(15)+\beta H_{10}C_5C_6(12)$
49	1101	1058			29.93	0.32	$\nu C_{18}C_{20}(12)+\nu C_{14}C_{16}(16)+\beta H_{15}C_{14}C_{16}(15)$
50	1074	1032	1042w	1030vw	4.91	0.12	$\nu C_{29}C_{25}(15)+\nu O_{32}C_{33}(50)$
51	1048	1007			0.05	0.44	$\nu C_5C_4(12)+\nu C_6C_5(30)+\beta H_8C_3C_4(22)$
52	1030	990		998w	6.58	0.01	$\tau H_{13}C_{12}C_1C_2(40)+\tau H_{19}C_{18}C_{20}C_{22}(45)$
53	1021	981			0.01	0.05	$\tau H_{13}C_{12}C_1C_2(35)+\tau H_{19}C_{18}C_{20}C_{22}(42)$
54	1015	975	977w		0.55	3.14	$\nu C_5C_4(12)+\nu C_6C_5(10)+\beta C_4C_3C_2(40)+\beta C_6C_1C_{12}(15)$
55	1009	969			0.46	2.04	$\nu C_{23}C_{22}(25)+\nu C_{22}C_{24}(15)+\beta C_{29}C_{25}C_{23}(55)$
56	1000	961			0.12	0.01	$\tau H_7C_2C_1C_6(10)+\Gamma C_4C_3C_5H_9(13)+\Gamma C_5C_4C_6H_{10}(55)$
57	985	946			0	0	$\tau H_7C_2C_1C_6(55)+\tau H_{11}C_6C_1C_2(20)+\Gamma C_5C_4C_6C_1(10)$
58	985	946			0.58	1.59	$\nu C_1C_{12}(10)+\nu C_{16}C_{18}(35)+\beta C_{16}C_{18}C_{20}(15)$
59	975	937			0.02	0.01	$\Gamma H_{28}C_{24}C_{27}C_{29}(22)+\Gamma H_{30}C_{27}C_{29}C_{25}(58)+\Gamma H_{31}C_{29}C_{27}C_{24}(10)$
60	944	907			2.38	0.27	$\nu C_{29}C_{25}(12)+\nu C_1C_{12}(25)+\nu O_{32}C_{33}(16)$
61	934	898			0.06	0.01	$\Gamma C_4C_3C_5H_9(39)+\tau H_{11}C_6C_1C_2(18)+\Gamma C_{14}C_{12}C_{16}H_{15}(15)+\Gamma C_5C_4C_6C_1(11)$
62	919	883			1.45	0.03	$\Gamma C_{18}C_{16}C_{14}H_{15}(18)+\tau H_{21}C_{20}C_{22}C_{23}(40)+\Gamma C_{16}C_{18}C_{14}O_{17}(12)$
63	894	858			1.39	0.08	$\Gamma C_{18}C_{16}C_{14}H_{15}(14)+\tau H_{26}C_{23}C_{25}O_{32}(35)+\Gamma C_{29}C_{27}C_{24}H_{28}(20)+\Gamma C_{24}C_{27}C_{29}H_{31}(15)$
64	884	850		848vw	0.64	0	$\tau H_{26}C_{23}C_{25}O_{32}(45)+\Gamma C_{29}C_{27}C_{24}H_{28}(18)+\Gamma C_{24}C_{27}C_{29}H_{31}(28)$
65	864	830			0.12	0.56	$\Gamma C_{18}C_{16}C_{14}H_{15}(22)+\tau H_{21}C_{20}C_{22}C_{23}(30)+\Gamma C_{24}C_{27}C_{29}H_{31}(10)$
66	861	827			0.29	0.53	$\nu C_2C_1(26)+\nu C_{14}C_{16}(15)$

Volume : 5 | Issue : 8 | August 2015 | ISSN - 2249-555X

67	849	816			0.01	0.03	$\tau H_8C_3C_4C_5(62)+\tau H_{11}C_6C_1C_2(28)$
68	790	759	780vw		7.15	0	$\Gamma H_{28}C_{24}C_{27}C_{29}(12)+\Gamma H_{30}C_{27}C_{29}C_{25}(20)+\Gamma H_{31}C_{29}C_{27}C_{24}(25)$
69	783	753			0.73	1.16	$\nu O_{32}C_{25}(20)+\beta C_{18}C_{16}O_{17}(15)$
70	773	743			0.28	0	$\Gamma C_6C_5C_4H_9(15)+\Gamma C_1C_6C_5H_{10}(12)+\Gamma C_5C_4C_6C_1(20)$
71	724	696	699w		1.56	0.29	$\nu C_{22}C_{24}(15)+\beta C_{18}C_{16}O_{17}(20)+\beta C_{23}C_{22}C_{24}(16)$
72	720	691			6.3	0.01	$\Gamma C_1C_6C_5H_{10}(15)+\Gamma C_{16}C_{18}C_{14}O_{17}(30)$
73	697	669			0.69	0	$\tau H_{11}C_6C_1C_2(10)+\Gamma C_5C_4C_6C_1(18)+\Gamma C_3C_2C_4C_5(12)+\tau C_{25}C_{23}C_{29}C_{27}(20)$
74	682	655			1.58	0.01	$\tau C_{25}C_{23}C_{29}C_{27}(50)+\Gamma C_{16}C_{14}C_{18}O_{17}(18)$
75	634	609		619vw	0.03	0.51	$\beta C_{18}C_{20}C_{22}(26)+\beta C_5C_4C_3(15)+\beta C_4C_3C_2(12)+\beta C_6C_1C_{12}(30)$
76	601	577			0.45	0.13	$\beta C_6C_5C_4(15)+\beta C_{23}C_{22}C_{24}(40)$
77	594	571			0	0.01	$\tau C_{27}C_{29}C_{24}C_{22}(46)+\tau C_{27}C_{29}C_{25}O_{32}(28)$
78	581	559			3.12	0.28	$\beta C_{18}C_{20}C_{22}(15)+\beta C_{24}C_{27}C_{29}(12)+\beta C_{33}O_{32}C_{25}(12)$
79	553	532			6.67	0.29	$\beta C_{18}C_{16}O_{17}(18)+\beta C_5C_4C_3(18)+\beta C_{23}C_{22}C_{24}(12)+\beta C_{24}C_{27}C_{29}(42)$
80	533	512			0.36	1.74	$\beta C_{24}C_{27}C_{29}(15)+\beta C_{23}C_{22}C_{24}(45)$
81	498	479			0.87	0	$\tau H_8C_3C_4C_5(15)+\Gamma C_3C_2C_4C_5(15)+\Gamma C_{12}C_1C_6C_2(40)$
82	458	440	455s	454vvw	0.53	0.01	$\tau C_{22}C_{24}C_{23}C_{25}(65)+\tau C_{20}C_{23}C_{24}C_{22}(15)$
83	456	438	430w		0.26	0.17	$\beta C_{24}C_{27}C_{29}(10)+\beta C_{20}C_{22}C_{24}(15)+\beta C_{29}C_{25}O_{32}(25)$
84	412	395	400w	404vw	0.01	0	$\tau H_7C_2C_1C_6(12)+\Gamma C_4C_3C_5C_6(38)+\Gamma C_3C_2C_4C_5(42)$
85	410	393			0.69	0.3	$\beta C_{33}O_{32}C_{25}(20)$
86	284	273			0.18	0.04	$\tau C_{27}C_{29}C_{24}C_{22}(25)+\tau C_{16}C_{18}C_{20}C_{22}(16)+\tau C_{20}C_{23}C_{24}C_{22}(22)$
87	279	268			0.39	0.61	$\beta C_{20}C_{22}C_{24}(10)+\beta C_{29}C_{25}O_{32}(18)+\beta C_{33}O_{32}C_{25}(38)$
88	277	266			0.08	0.1	$\Gamma C_4C_3C_5C_6(35)+\Gamma C_3C_2C_4C_5(15)+\tau C_{14}C_{16}C_{18}C_{20}(15)$
89	268	258			0.44	0.18	$\beta C_{12}C_{14}C_{16}(25)+\beta C_6C_5C_4(10)+\beta C_1C_{12}C_{14}(18)$
90	263	253			0.02	0.03	$\tau H_{36}C_{33}O_{32}C_{25}(45)+\tau C_{22}C_{24}C_{23}C_{25}(12)+\tau C_{25}C_{29}C_{23}O_{32}(20)$
91	209	200		220vw	0.1	0.49	$\beta C_{20}C_{22}C_{24}(32)+\beta C_{29}C_{25}O_{32}(22)+\beta C_{33}O_{32}C_{25}(12)$
92	206	198			0	0.27	$\tau H_{36}C_{33}O_{32}C_{25}(35)+\tau C_{25}C_{29}C_{23}O_{32}(40)$
93	179	172			0.01	0.44	$\tau C_{18}C_{20}C_{22}C_{23}(30)+\tau C_{14}C_{16}C_{18}C_{20}(40)$

94	176	169			0.03	0.17	$\beta C_{12}C_{14}C_{16}(20)+\beta C_{20}C_{22}C_{24}(15)+\beta C_{16}C_{18}C_{20}(12)$
95	109	104			0.21	0.12	$\tau C_{16}C_{18}C_{20}C_{22}(22)+\tau C_{33}O_{32}C_{25}C_{23}(18)+\tau C_{20}C_{23}C_{24}C_{22}(20)$
96	97	93			0.02	0.19	$\beta C_6C_5C_4(22)+\beta C_{16}C_{18}C_{20}(46)$
97	88	84			0.12	0.57	$\tau C_{14}C_{16}C_{18}C_{20}(18)+\tau C_{33}O_{32}C_{25}C_{23}(28)+\Gamma C_{12}C_1C_6C_2(15)$
98	78	75		70s	0.28	0.21	$\tau C_{12}C_{14}C_{16}C_{18}(22)+\tau C_{14}C_{12}C_1C_6(15)+\tau C_1C_{12}C_{14}C_{16}(35)$
99	60	57			0.11	0.82	$\tau C_{16}C_{18}C_{20}C_{22}(15)+\tau C_{33}O_{32}C_{25}C_{23}(36)+\tau C_{20}C_{23}C_{24}C_{22}(25)$
100	32	31			0.05	1.85	$\beta C_5C_4C_3(35)+\beta C_{14}C_{16}C_{18}(55)$
101	21	21			0.15	1.89	$\tau C_{18}C_{20}C_{22}C_{23}(36)+\tau C_{14}C_{12}C_1C_6(32)+\tau C_1C_{12}C_{14}C_{16}(18)$
102	19	18			0.05	4.14	$\tau C_{12}C_{14}C_{16}C_{18}(52)+\tau C_{14}C_{12}C_1C_6(18)+\tau C_{16}C_{18}C_{20}C_{22}(20)$
					0.85	0.29	$\nu C_{29}H_{31}(91)$

W-weak, vw-very weak, vvw-very very weak, Abs-absolute, Rel-relative, Scale factor: 0.9608 [21].

a Relative IR absorption intensities normalized with highest peak absorption equal to 100,

bRelative Raman intensities calculated by Equation (1) and normalized to 100.

cTotal energy distribution calculated at B3LYP/6-311++G(d,p) level.

4.2.2 C=O and C–O vibrations

It has long been known that the vibrational frequency of a carbonyl group varies according to the class of compound in which it occurs. This multiple bonded group is highly polar and therefore gives rise to an intense infrared (IR) absorption band. The carbon–oxygen double bond is formed by Pπ–Pπ bonding between carbon and oxygen inter-molecular hydrogen (H) bonding, reduces the frequencies of the C=O stretching absorption to a greater degree than does inter- molecular H bonding because of the different electro negatives of C and O, the bonding are not equally distributed between two atoms. The loan pair of electrons on oxygen also determines the nature of the carbonyl group. Normally carbonyl group vibrations occur in the region 1850–1600 cm^{-1} [34]. In our present study, the weak band observed at 1654 cm^{-1} in FT-IR spectrum is corresponds to the carbonyl stretching frequency of the title compound. The theoretical calculations predict the C=O stretching vibrational mode at 1659 cm^{-1} (mode no. 17) by B3LYP/6-311++G(d,p) method as shown in Table 2. The reported value of 1654 cm^{-1} for the C=O stretching vibration in our title molecule is below the expected range and may be due to the conjugation of the C=O bond with the aromatic ring which may increase its single bond character, resulting in lowered values of carbonyl-stretching wavenumbers [35]. Sudha et al., [18] observed C=O stretching vibrations at 1650 cm^{-1} in FT-IR and 1651 cm^{-1} in FT-Raman for (*1E,4E*)-1-(3-Nitrophenyl)-5-phenylpenta-1,4-dien-3-one, which support our present assignment.

The C=O stretching vibration is mixed with the C=C and C–C stretching vibrations. As evident from Table 2, the maximum TED contribution of this mode is 51%. The in-plane/out-of-plane bending modes of C-C=O lies in the mode nos: 71/72, in which mode no: 71 is in line with observed FT-IR band (699 cm^{-1}). As revealed by PED, the peaks identified at 1259/1042 cm^{-1} in FTIR and calculated at 1263/1032 cm^{-1} (mode no: 37/50) are assigned to νC_{25}-O_{32}/νC_{33}-O_{32} modes, respectively. This assignment is supported by the observed bands at 1259 cm^{-1} (FTIR)/1042: FTIR and 1030 cm^{-1}: FT-Raman and also find support from literature [36]. The $\beta_{C\text{-}O}$, $\Gamma_{C\text{-}O}$ and β_{COC}, Γ_{COC} are calculated at 438, 253 cm^{-1} (mode nos: 83, 90) and 268, 253 cm^{-1} (mode nos: 87, 90), respectively. According to TED results, these modes are mixed with β_{CCC} and Γ_{CCC} modes.

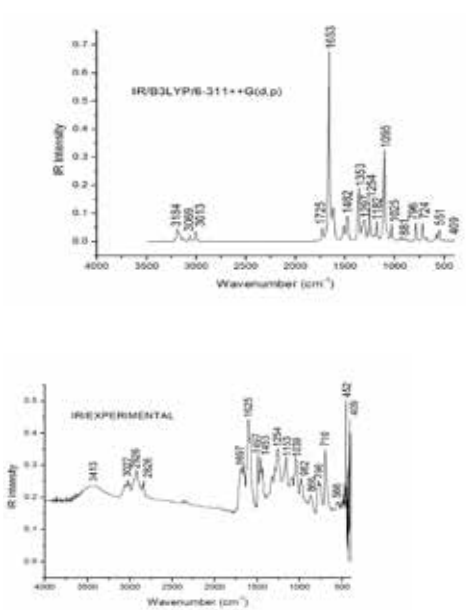

Figure.2 The combined theoretical and experimental FT-IR spectra of MPPDO.

Volume : 5 | Issue : 8 | August 2015 | ISSN - 2249-555X

4.2.3 C-H vibrations

The hetero aromatic structure shows the presence of C–H stretching vibration in the region of 3100–3000 cm^{-1}, which is the characteristic region for the ready identification of C–H stretching vibration [37]. In this region, the bands are not affected appreciably by the nature of the substituents. The C–H stretching modes usually appear with strong Raman intensity and are highly polarized, may be owing to this high polarization, Raman bands have not been observed in the experimental spectrum. In IR spectra, most of the aromatic compounds have nearly four peaks in the region 3080–3010 cm^{-1} due to ring C−H stretching bands. IR frequencies of C−H bands are a function of sp hybridization [38]. The scaled vibrations, [mode nos: 11, 10, 8-6, 4-1] assigned to the aromatic C−H stretching computed in the range 3035–3082 cm^{-1} by B3LYP/6-311++G(d,p) method shows good agreement with the recorded weak Raman band at 3060 cm^{-1}. The TED corresponding to these vibrations are pure mode (>80%).

The C–H in-plane bending frequencies appear in the range of 1000–1300 cm^{-1} and are very useful for characterization purposes [37]. In our present study, the C−H in-plane bending vibrations appear as very weak to weak FT-IR and FT-Raman bands in the range 1096-1489 cm^{-1} and 1081-1450 cm^{-1} respectively, which show good correlation with computed wavenumbers by B3LYP method in the range 1466-1007 cm^{-1} (mode nos: 24,25, 29, 31, 37, 42, 43, 47, 51). The TED values confirm that these vibrations are of mixed mode as it is evident from Table 2 and their contributions in the range 22-72%. The out-of-plane bending vibrations occur in the wavenumber range 800–1000 cm^{-1} [39]. The C−H out-of-plane bending vibrations of the MPPDO are well identified at 743, 759, 830, 850, 858, 898, 937, 946 and 961 cm^{-1} (mode nos: 70, 68, 65, 64, 63, 67, 59, 57, 56), in which mode nos: 64 & 38 are in line with observed spectral values (848 cm^{-1}/Raman and 780 cm^{-1}/FT-IR). The ν_{C-H} and β_{C-H} vibrations of carbon chains show weak bands at 3026 cm^{-1} (FT-IR) and 1275, 1182 cm^{-1} (FT-Raman) respectively. The calculated frequencies (mode nos: 5, 11-13 and 35, 36, 39, 40) are matched well with the experimental values. The mode nos: 61-63, 65 are attributed to ΓCH mode. These assignments are in line with the ranges given in the above literatures.

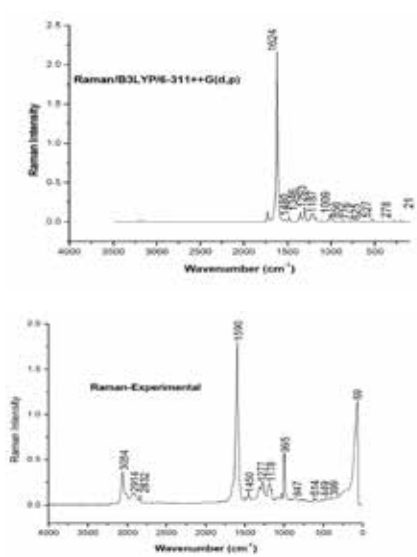

Figure.3 The combined theoretical and experimental FT-Raman spectra of MPPDO

4.2.4 Ring vibrations

The ring C=C and C−C stretching vibrations, known as semicircle stretching usually occur in the region 1400–1625 cm^{-1} [40, 41]. In general, the bands are of variable intensity and are observed at 1625–1590, 1590–1575, 1540–1470, 1460–1430 and 1380–1280 cm^{-1} from the frequency ranges given by Varsanyi [37] for the five bands in the region. Zhang et al., [42] reported the aromatic C=C stretching vibrations at 1488, 1436 and 1409 cm^{-1} for N-(2-hydroxybenzylidene)acetohydrazide. Hence in our present study, the C−C stretching vibrations of aromatic rings are assigned to harmonic frequencies: 1299, 1303, 1306, 1410, 1421, 1455, 1547, 1549, 1560 and 1581 (mode nos: 34-32, 30, 29, 25, 23-21, 19). The weak band observed at 1451 cm^{-1} in FT-IR and very weak band at 1450 cm^{-1} in FT-Raman spectra shows good agreement with mode no: 25.

Symmetrical benzene ring breathing vibration is allowed in the Raman scattering, but is forbidden in IR absorption. It is predicted at 988 cm^{-1} and is observed in the Raman spectrum of benzene at 993 cm^{-1} [43]. In the MPPDO molecule, the ring breathing vibration mixed with β_{CH} vibration and assigned to mode no: 51/1007 cm^{-1}. In benzene, the fundamentals (997 cm^{-1}) and (1010 cm^{-1}) represents the ring breathing and trigonal bending modes, respectively, gives rise to combined modes in molecules belonging to the reduced symmetry. As the energies of these vibrations are very close, there is an appreciable interaction between these vibrations, and consequently their energies will be modified. Further, these modes are drastically affected in magnitude upon substitution [44]. Based on the above factors, in our present study the calculated frequencies 969 and 975 cm^{-1} (mode nos: 55 & 54) are assigned to trigonal bending modes of phenyl rings. This assignment is in agreement with the band observed at 977 cm^{-1} in FT-IR spectrum. Two bands usually observed are those due to the in-plane and out-of-plane ring deformation vibrations. In general, the in-plane deformation assigned at higher frequency than the out-of-plane deformation and also appeared as weak band for mono and para substituted benzenes. They are often masked by other stronger absorptions which may occur due to the substituent groups [45]. For the title molecule, the C−C−C in-plane bending vibrations for both rings are observed at 699/619 cm^{-1} in FT-IR and FT-Raman spectra respectively and their corresponding harmonic values are: 696/609 cm^{-1} (mode nos: 71/75). The C−C−C out-of-plane bending vibrations computed by B3LYP method at 395, 743 cm^{-1} (mode nos: 84, 70). One of the Γ_{CCC} deformations generate band at 400/404 cm^{-1} in FT-IR/FT-Raman spectra and these assignments find support from literature [46].

The $\nu_{C=C}$ and ν_{C-C} vibrations of carbon-carbon chain in between the two rings are identified and assigned in this study. The vibrational assignments of $\nu_{C=C}$ and ν_{C-C} vibrational modes are completely made on the basis of TED, because they have not identified in the recorded frequency region except for $C_{18}=C_{20}$ a medium intensity band at 1601 cm^{-1} in FTIR spectrum. The corresponding Raman counterpart observed at 1598 cm^{-1} as a very strong band. The mode nos: 20 and 38, 40, 48, 58 are attributed to $\nu(C_{12}=C_{14})$ and $\nu(C_1-C_{12})$, $\nu(C_{20}-C_{22})$, $\nu(C_{14}-C_{16})$, $\nu(C_{16}-C_{18})$ modes respectively. The mode no: 40 is further supported by observed Raman band: 1182 cm^{-1}. The harmonic frequencies 946 and 609/619 cm^{-1}: FT-Raman (Mode nos: 58 & 75) are belongs to $\beta C_{16}-C_{18}=C_{20}$ and $\beta C_{18}=C_{20}-C_{22}$ modes, respectively.

4.3 Natural Bond Orbital (NBO) Analysis

Volume : 5 | Issue : 8 | August 2015 | ISSN - 2249-555X

The NBO analysis carried out for the title molecule in order to understand various second-order interactions between the filled orbital of one subsystem and vacant orbital of another subsystem, which is a measure of the inter-molecular delocalization or hyperconjugation. NBO analysis provides the most accurate possible 'natural Lewis structure' picture of 'j' because all orbital details mathematically chosen to include the highest possible percentage of the electron density. A useful aspect of the NBO method is that it gives information about interactions of both filled and virtual orbital spaces that could enhance the analysis of intra- and inter-molecular interactions. The hyperconjugation may be given as stabilizing effect that arises from an overlap between an occupied orbital with another neighboring electron deficient orbital when these orbitals are properly orientation. This non-covalent bonding–antibonding interaction can be quantitatively described in terms of the NBO analysis, which is expressed by means of the second-order perturbation interaction energy ($E^{(2)}$) [47-50]. This energy represents the estimation of the off-diagonal NBO Fock matrix elements. It can be deduced from the second-order perturbation approach [51].

$$E^{(2)} = \Delta E_{ij} = q_i \frac{F(i,j)^2}{\varepsilon_j - \varepsilon_i}$$

Where, q_i is the donor orbital occupancy, ε_i and ε_j are diagonal elements (orbital energies) and *F(i, j)* is off diagonal NBO Fock matrix elements. In NBO analysis large $E^{(2)}$ value shows the intensive interaction between electron donors and electron-acceptors and greater the extent of conjugation of the whole system, the possible intensive interactions are given in Table 3. The second-order perturbation theory analysis of Fock matrix in NBO basis shows strong intra-molecular hyper-conjugative interactions of π electrons. NBO analysis has been performed on the molecule at the DFT/B3LYP/6-311++G(d,p) level in order to elucidate the intra-molecular, rehybridization and delocalization of electron density (ED) within the molecule. The magnitude of charge transfer is higher from the lone pair of atom than from overlapping bond orbitals. The larger ED of bonding orbital (Lewis) with lower occupancy of antibonding orbital stabilize less energy and vice versa. The lewis and non-lewis NBO'S of MPPDO are in Table S1 (Supporting information).

The intra-molecular hyper-conjugative interactions are formed by the orbital overlap between π→π* bond orbital which results inter-molecular charge transfer (ICT) and causing stabilization of the system. The strong intra-molecular hyperconjugative interaction $\pi(C_{16}-O_{17})\rightarrow\pi^*(C_{18}-C_{20})$ which increase the ED (0.077e) that weakens the respective bonds leading to stabilization of 128.53 kJ/mol. Similarly interaction from $\pi C_{16}-O_{17}\rightarrow\pi^*C_{12}-C_{14}$ with ED (0.078e) leading to the stabilization of 122.21 kJ/mol. The C_1-C_2 bond has ED (1.975e) transfer energy 17.07 and 14.39 kJ/mol to the acceptor orbital of C_1-C_6 and C_2-C_3, respectively having ED 0.022e and 0.016e. The occupancy of O_{32} is (1.959e) and the stabilization energy $E^{(2)}$ coupled with hyperconjugative interactions $n1(O_{32})\rightarrow(C_{23}-C_{25})$, $(C_{25}-C_{29})$ are 24.39 and 27.28 kJ/mol, respectively. The orbitals interaction between $\pi(C_{22}-C_{24})\rightarrow\pi^*(C_{27}-C_{29})$, $\pi(C_{27}-C_{29})\rightarrow\pi^*(C_{23}-C_{25})$, $\pi(C_{23}-C_{25})\rightarrow\pi^*(C_{22}-C_{24})$ are 87.78, 92.42, 88.70 kJ/mol, respectively (Table S1). These increasing interaction energies are due to the strong ICT interactions leading to the stabilization. The ED of the six conjugated double bonds of the two-phenyl rings (~1.66e) clearly explain the strong delocalization in MPPDO. The orbitals interaction between $\pi(C_{18}-C_{20})\rightarrow\pi^*(C_{16}-O_{17})$, $\pi^*(C_{22}-C_{24})$ are 71.42 and 41.21 kJ/mol which explain that the energy transfer occur between the phenyl ring and carbonyl group through conjugation, which are also responsible for stabilization of the MPPDO molecule.

The NBO analysis also describes the bonding in terms of the natural hybrid orbital, n2 (O_{17}) which occupy a lower energy orbital (-0.2531e) with considerable p-character (99.95%) and low occupation number (1.8892e). Similarly n1 (O_{32}) occupy a lower energy orbital (-0.3024e) with p-character (99.80%) and higher occupation number (1.9593e). Also n2 (O_{32}), which occupy a higher energy orbital (-0.5852e) with considerable p-character (52.52%) and lower occupation number (1.9543e) and the other n1 (O_{17}) occupy a higher energy orbital (-0.6872e) with p-character (39.57%) and with higher occupation number (1.9792e). Thus a very close to pure p-type lone pair orbital participates in electron donation to the π*(C–C) orbital for n(O)→π*(C–C) interactions in the compound MPPDO. The strong intra-molecular hyperconjugative interactions from $\pi(C_{16}-O_{17})\rightarrow\pi^*(C_{18}-O_{20})$ exhibits the sp^1 hybridization with 100% p-character and this bond is essentially controlled by the p-character of these hybrid orbitals.

Table. 3 Second order perturbation theory analysis of Fock matrix in NBO basis for MPPDO using B3LYP/6-311++G(d,p) basis set.

Type	**Donor NBO (i)**	ED/e	Acceptor NBO (j)	ED/e	$E^{(2)}$ kJ/mol	E(j)– E(i) a.u.	F(i,j) **a.u.**
σ - σ*	C1–C2	1.974	C1–C6	0.021	17.07	1.26	0.064
σ - σ*			C2–C3	0.016	14.39	1.26	0.059
π - π*	C2–C3	1.671	C1–C6	0.364	86.99	0.28	0.069
π - π*			C4–C5	0.325	84.89	0.28	0.067
π - π*	C1–C6	1.631	C2–C3	0.308	81.43	0.28	0.067
π - π*	C4–C5	1.657	C1–C6	0.364	83.39	0.28	0.067
π - π*			C2–C3	0.308	83.14	0.28	0.067
π - π*	C12–C14	1.857	C1–C6	0.364	40.46	0.3	0.051
π - π*			C16–O17	0.207	72.72	0.28	0.064
π - π*	C16–O17	1.969	C12–C14	0.078	14.64	0.39	0.033

Volume : 5 | Issue : 8 | August 2015 | ISSN - 2249-555X

π - π*			C18–C20	0.077	14.90	0.39	0.033
π - π*	C18–C20	1.859	C16–O17	0.207	71.42	0.28	0.063
π - π*			C22–C24	0.368	41.21	0.3	0.052
σ - σ*	C22–C24	1.975	C22–C23	0.023	16.99	1.26	0.064
π - π*	C22–C24	1.633	C18–C20	0.077	48.66	0.29	0.056
π - π*			C23–C25	0.338	81.42	0.28	0.066
π - π*			C27–C29	0.333	87.78	0.28	0.068
π - π*	C23–C25	1.666	C22–C24	0.368	88.70	0.29	0.071
π - π*			C27–C29	0.333	81.13	0.29	0.066
π - π*	C27–C29	1.666	C22–C24	0.368	78.74	0.29	0.066
π - π*			C23–C25	0.338	92.42	0.28	0.07
π - π*	O32–C33	1.977	C23–C25	0.338	13.01	0.77	0.047
n - π*	LP(2) O17	1.889	C14–C16	0.059	72.51	0.64	0.095
			C16–C18	0.059	72.72	0.64	0.095
n - σ*	LP(1) O32	1.959	C23–C25	0.030	24.39	0.86	0.063
			C25–C29	0.030	27.28	0.86	0.067
π - π*	C16–O17	0.207	C12–C14	0.078	122.21	0.03	0.064
π - π*	C16–O17	0.207	C18–C20	0.077	128.53	0.02	0.064

4.4 Molecular Electrostatic Potential (MEP):

MEP and electrostatic potential are useful quantities to illustrate the charge distributions of molecules and used to visualize the various charged regions of a molecule. Therefore, the charge distributions can give information about how the molecules interact with another molecule. MEP is widely used as a reactivity map displaying most probable regions for the electrophilic attack of charged point-like reagents on organic molecules [52]. Molecular MEP at a point in space around a molecule gives information about the net electrostatic effect produced at that point by total charge distribution (electron + proton) of the molecule and correlates with dipole moments, electronegativity, partial charges and chemical reactivity of the molecules. It provides a visual method to understand the relative polarity of the molecule. An ED iso surface mapped with electrostatic potential surface depicts the size, shape, charge density and site of chemical reactivity of the molecules.

MEP is related to the ED and is a very useful descriptor in understanding sites for electrophilic and nucleophilic reactions as well as hydrogen bonding interactions [53, 54]. The different values of the electrostatic potential at the surface are represented by different colors; red represents regions of most electronegative electrostatic potential, blue represents regions of the most positive electrostatic potential and green represents region of zero potential. Potential increases in the order red < orange < yellow < green <blue. Such mapped electrostatic potential surface have been plotted for title molecule MPPDO using B3LYP/6-311++G(d,p) basis set. The negative region is localized on the oxygen atom and the positive region is localized on the hydrogen atoms. These results provide information about the region where the compound can interact inter-molecularly and make bond metallically. The neutral sites of the molecule are indicated by the green region. This predict the most reactive site for both electrophilic and nucleophilic attack. The MEP diagram is shown in Figure 4.

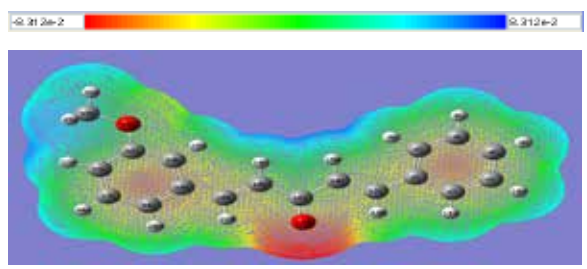

Figure. 4 The molecular electrostatic potential surface of MPPDO.

4.5 Non-Linear Optics (NLO)

The first hyperpolarizabilities (β_0, α_0 and $\Delta\alpha$) of MPPDO are calculated using B3LYP/6-311++G(d,p) basis set, based on the finite-field approach. In the presence of an applied electric field, the energy of a system is a function of the electric field. First hyperpolarizability is a third rank tensor that can be described by a 3x3x3 matrix. The 27 components of the 3D matrix can be reduced to 10 components due to Kleinman symmetry [55]. It can be given in the lower tetrahedral format. It is obvious that the lower part of the 3x3x3 matrix is a tetrahedral. The components of V are defined as the coefficients in the Taylor series expansion of the energy in the external electric field. When the external electric field is weak and homogeneous, this expansion becomes:

$$E = E^0 - \mu_\alpha F_\alpha - 1/2\alpha_{\alpha\beta}F_\alpha F_\beta - 1/6\beta_{\alpha\beta\gamma}F_\alpha F_\beta F_\gamma \qquad (3)$$

Where $E^0$is the energy of the unperturbed molecules, F_α is the field at the origin, and $\mu_\alpha, \alpha_{\beta}, \beta_{\alpha\beta\gamma}$ are the components of the dipole moment, polarizability and the first hyperpolarizabilities, respectively. The total static dipole moment μ, the mean polarizability α_0, the anisotropy of polarizability $\Delta\alpha$ and the mean first hyperpolarizability β_0, using the x, y, z components are defined as [60]

Volume : 5 | Issue : 8 | August 2015 | ISSN - 2249-555X

$$\mu = (\mu_x^2 + \mu_y^2 + \mu_z^2)^{1/2} \quad (4)$$

$$\alpha_0 = \frac{\alpha_{xx} + \alpha_{yy} + \alpha_{zz}}{3} \quad (5)$$

$$\Delta\alpha = 2^{-1/2}\left[(\alpha_{xx} - \alpha_{yy})^2 + (\alpha_{yy} - \alpha_{zz})^2 + (\alpha_{zz} - \alpha_{xx})^2 + 6(\alpha_{xy}^2 + \alpha_{yz}^2 + \alpha_{xz}^2)\right]^{1/2} \quad (6)$$

$$\beta_0 = \left(\beta_x^2 + \beta_y^2 + \beta_z^2\right)^{1/2} \quad (7)$$

Many organic molecules, containing conjugated π electrons are characterized by large values of molecular first hyperpolarizabilities, were analyzed by means of vibrational spectroscopy [57-60]. The intra-molecular charge transfer from the donor to acceptor group through a single-double bond conjugated path can induce large variations of both the molecular dipole moment and the molecular polarizability, making IR and Raman activity strong at the same time [61].

Theoretical investigation plays an important role in understanding the structure–property relationship, which is able to assist in designing novel NLO materials. It is well known that the higher values of dipole moment, molecular polarizability, and hyperpolarizability are important for more active NLO properties. The present study reveals that the π-π interaction can make larger intra-molecular interaction and hence the polarizability of the molecule increases. It is evident from Table 4, the molecular dipole moment (μ), molecular polarizability (α) and hyperpolarizability (β_0) are calculated about 1.5027 (D), 0.7376x10^{-30} esu and 18.3707 x10^{-30} esu, respectively. They clearly reveal that the molecule has more nonlinear optical activity; its electronic transition shown at 351nm which also emphasis the optical behavior and very closer gap between valence and conduction band. The β_0 value of the title compound is forty nine times greater than that of urea. Hence the title molecule MPPDO has good NLO activity.

Table. 4 The Non-linear optical properties of MPPDO.

Parameters	B3LYP/6-311++G(d,p)
Dipole moment	Debye
μ_x	-0.7216
μ_y	1.3182
μ_z	0.0002
μ	1.5028 Debye
Polarizability	x10^{-30}esu
α_{xx}	467.4603
α_{xy}	14.7482
α_{yy}	231.0407
α_{xz}	-0.0025
α_{yz}	0.0027
α_{zz}	117.3899
α	0.7376x10^{-30} esu
Hyperpolarizability	x10^{-30} esu
β_{xxx}	990.0123
β_{xxy}	-1734.9335
β_{xyy}	-269.2127
β_{yyy}	-281.6752
β_{xxz}	-0.2682
β_{xyz}	-0.0286
β_{yyz}	-0.0067
β_{xzz}	-30.3816
β_{yzz}	5.4013
β_{zzz}	0.0322
β_0	18.3707 x10^{-30}esu

Standard value for urea (μ=1.3732 Debye, β_0=0.3728x10^{-30}esu)

4.6 Frontier molecular orbital analysis

The energies of the highest occupied molecular orbital (HOMO) and the lowest unoccupied molecular orbital (LUMO) are computed at the B3LYP/6-311++G(d,p) level. HOMO and LUMO orbitals and there corresponding energies are shown in Figure 5 and values are listed in Table 5 respectively. Generally, the energy values of LUMO and HOMO and the energy gap reflect the chemical activity of the molecule. HOMO as an electron donor represents the ability to donate an electron, while LUMO as an electron acceptor represents the ability to obtain an electron. The energy gap between HOMO and LUMO determines the kinetic stability, chemical reactivity and optical polarizability and chemical hardness–softness of a molecule [62].

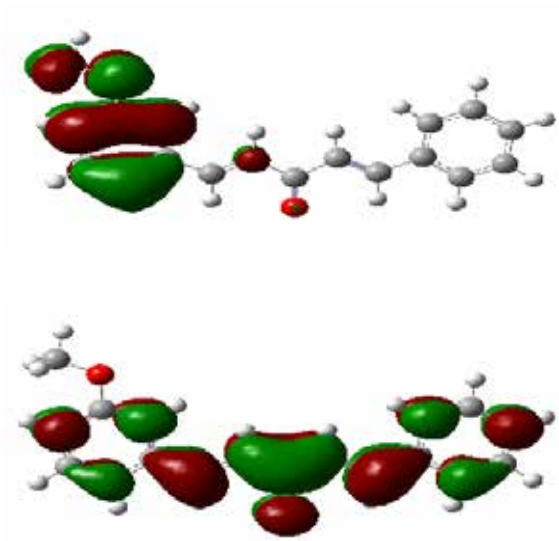

Lumo = -2.6464 eV

Figure. 5 The frontier molecular orbital of MPPDO

The HOMO is located over mainly on methoxy group and the atoms in methoxy phenyl ring. The HOMO energy is -6.4055 eV. The LUMO is located all over the molecule except on methoxy group and the energy is -2.6464 eV.

HOMO = -6.4055 eV
LUMO = -2.6464 eV
ΔE = 3.7591 eV

The calculated HOMO and LUMO energies clearly show that the charge transfer occurs within the molecule.

Volume : 5 | Issue : 8 | August 2015 | ISSN - 2249-555X

Table .5 The Frontier molecular orbitals of MPPDO.

Occupancy	Orbital energies a.u.	Orbital energies eV	Kinetic energies a.u.
O66	-0.2698	-7.3434	1.1187
O67	-0.2520	-6.8585	2.3149
O68	-0.2465	-6.7083	1.4297
O69	-0.2414	-6.5693	1.3488
O70	-0.2354	-6.4055	1.3882
V71	-0.0972	-2.6464	1.3989
V72	-0.0513	-1.3975	1.2898
V73	-0.0255	-0.6941	1.2449
V74	-0.0162	-0.4410	1.3581
V75	-0.0137	-0.3733	0.2511

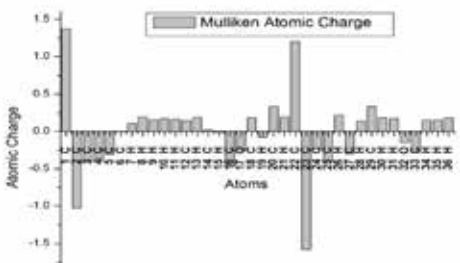

Figure. 6 The Mulliken atomic charges plot of MPPDO.

4.7 Mulliken charge analysis

The Mulliken population analysis in MPPDO molecule was calculated using B3LYP level with 6-311++G(d,p) basis set. The Mulliken charge distribution for the optimized structure of MPPDO is shown in Figure 6 and are listed in Table 6. The charge distribution on the molecule has a significant influence on the vibrational spectra. The Mulliken charge is directly related to the vibrational properties of the molecule, and quantifies how the electronic structure changes under atomic displacement; it is therefore related directly to the chemical bonds present in the molecule.

Mulliken atomic charge calculation has an important role in the application of quantum chemical calculation to molecular system [63]. The atom C_{23} has more negative charge (-1.5827 a.u) and the atoms C_1 and C_{22} have more positive charges (1.3725 a.u and 1.1974 a.u). All the hydrogen atoms of MPPDO show positive charge in the range of 0.1066 a.u - 0.2184 a.u. The hydrogen atoms attached to the carbon atoms C_{14} and C_{18} shows negative charge due to the net atomic charge of the adjacent carbonyl group.

Table. 6 The Mulliken atomic charges of MPPDO

Atoms	Mulliken Charges (a.u.)
1C	1.3725
2C	-1.0331
3C	-0.4088
4C	-0.3668
5C	-0.3080
6C	-0.0060
12C	0.1403
14C	0.0175
16C	-0.4704
17O	-0.2530
18C	0.1765
20C	0.3307
22C	1.1974
23C	-1.5827
24C	-0.2339
25C	-0.4114
27C	-0.3026
29C	0.3327
32O	-0.1522
33C	-0.2926

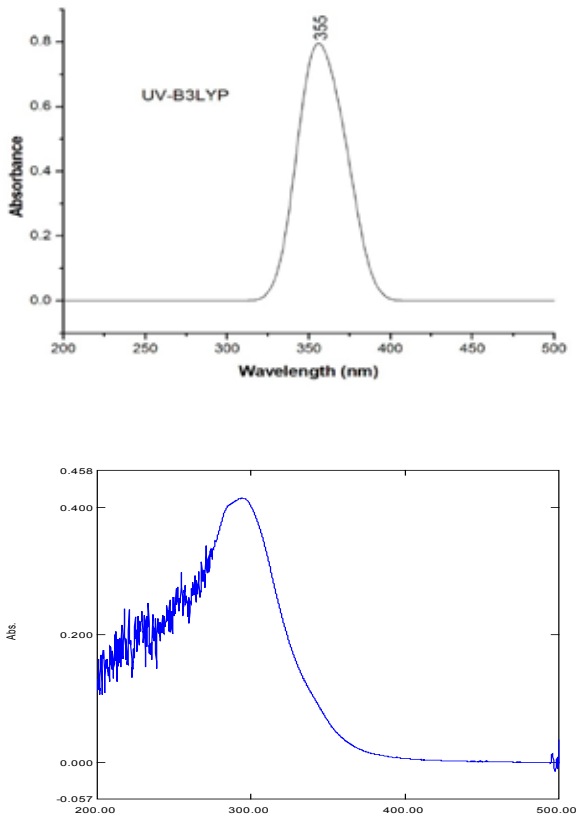

Figure. 7 The combined theoretical and experimental UV-Visible spectra of MPPDO

Table 7 The electronic transition of MPPDO.

Excited states	Oscillator strength	Calculated Band gap(eV/nm)	Experimental Band gap(eV/nm)
Excited State: 1	Singlet-A(f=0.0000)	2.9840 eV/415.49 nm	
67 → 71	0.6837	4.2121	
Excited State: 2	Singlet-A(f=0.4123)	3.3561 eV/369.43 nm	
68 → 71	-0.1557	-4.0619	
70 → 71	0.6518	3.7591	
Excited State: 3	Singlet-A(f=0.6589)	3.5233 eV/351.90 nm	294 nm
68 → 71	0.2858	4.0619	
69 → 71	0.5882	3.9229	
70 → 71	0.1298	3.7591	

4.8 UV Analysis

Electron transitions are usually classified according to the orbitals engaged or to specific parts of the molecule involved. In organic compounds the common types of electronic transitions are, $\sigma \rightarrow \sigma^*$, $n \rightarrow \pi^*$ and $\pi \rightarrow \pi^*$. The UV absorption spectrum of MPPDO is shown in Figure 7. The absorption maximum of MPPDO observed at 294 nm and this band is due to the $\pi \rightarrow \pi^*$ transition of the molecule. The intensity of the band is very high. The absorption maxima (351 nm) of MPPDO is calculated, by TD-DFT/6-311++G(d,p) method. The calculated results involving the vertical excitation energies, oscillator strength (f) and wavelength are carried out and are listed in Table 7. Typically, according to Frank-Condon principle, the

Volume : 5 | Issue : 8 | August 2015 | ISSN - 2249-555X

maximum absorption peak (λ_{max}) in a UV-Vis spectrum corresponds to vertical excitation. The absorption max 294 nm is in moderate agreement with theoretical absorption maxima (351 nm), difference experimental and theoretical value is due to solvent the effect. The peak absorbed at 294 nm shows that the molecule is highly conjugative, it will have more optical property.

5. Conclusion

The molecular structure and complete vibrational analysis have been carried out for MPPDO, based on the quantum chemical calculation and TED assignment. The difference between the observed and scaled wavenumber values of most of the fundamentals is very small. The most characteristic frequencies of the functional groups such as methoxy, methylene and carbonyl are assigned within their characteristic region. The hyperpolarizability of MPPDO is calculated about β_0 = 18.3707x10^{-30} esu, it clearly reveals that the molecule has more nonlinear activity; its electronic transition shown at 355nm is also emphasis optical behavior and very closer gap between valence and conduction band. The intra-molecular hyper-conjugative interactions are formed by the orbital overlap between $\pi \rightarrow \pi^*$ bond orbital which results ICT and causing stabilization of the system. The band gap energy is calculated about 3.7591 eV, which shows that more charge transfers occur within the molecule. MEP surface predict the most reactive site for both electrophilic and nucleophilic attack of MPPDO.

REFERENCE

Dhar, D. N. The Chemistry of Chalcones and Related Compounds New York: John Wiley (1981). | | [2] Dimmock, J.R., Elias, D.W., Beazely, M. A., Kandepu, N. M., Curr. Med. Chem. (1999) 6, 1125 –1149. | | [3] Satyanarayana, M. Tiwari, P., Tripathi, B. K., Sriwastava, A. K. Pratap, R., Bioorg. Med. Chem. (2004) 12, 883–887. | | [4] Sarojini, B. K., Narayana, B., Ashalatha, B. V., Indira, J., Lobo, K. G., J. Cryst. Growth, (2006) 295, 54 -59. | | [5] Samshuddin, S., Butcher, R. J., Akkurt, M., Narayana, B., Yathirajan, H. S., Sarojini, B. K., Acta Cryst. E67, (2011) o1954–o1955. | | [6] Samshuddin, S., Narayana, B., Sarojini, B. K., Khan, M. T. H, Yathirajan, H. S., Raj, C. G. D., | Raghavendra, R., Med. Chem. Res. (2011) doi: 10.1007/s00044-011-9735-9. | | [7] Samshuddin, S., Narayana, B., Shetty, D. N., Raghavendra, R., Der. Pharm. Chem. (2011) 3, 232-240. | | [8] Fun, H.K., Hemamalini, M., Samshuddin, S., Narayana, B., Yathirajan, H.S., Acta Cryst. E66, (2010) o582–o583. | | [9] Jasinski, J. P., Guild, C. J., Samshuddin, S., Narayana, B., Yathirajan, H., Acta Cryst. E66, (2010) o2018. | | [10] Baktır, Z. , Akkurt, M., Samshuddin, S., Narayana, B., & Yathirajan, H. S., Acta Cryst. E67, (2011) o1292–o1293. | [11] Gaussian 03W program, (Gaussian Inc., Walling ford CT) (2004). | [12] Schlegel. H.B., J. Comput. Chem. (1982) 3, 214-218. | [13] Michalska, D., Raint Program, Wroclaw University of Technology, Poland (2003). | [14] Michalska, D., Wysokinski, R., Chem. Phys. Lett. (2005) 403, 211-217. | [15] Baker, J., Jarzccki, A.A., Pulay, P., J. Phys. Chem. A (1998) 102, 1412-1424. | [16] Pulay, P., Baker, J. Wolinski. K., Green Arc Road, Suite a, Fayettevile, AR72703. USA. (2013). | [17] Samshuddin, S., Ray J. B, Akkurt M, Narayana, B., Sarojini B.K, Yathirajan, H. S., ActaCryst. E68, (2012) o74–o75. | | [18] Sudha, S, Sundaraganesan, N., Vanchinathan, K., Muthu, K., Meenakshisundaram, SP., Journal of Molecular Structure, (2012) 1030, 191–203. | | [19] Hendrik F. Hameka. J. Org. Chem., (1987) 52 (22), pp 5025–5026. | | [20] Jamroz, M. H., Vibrational Energy Distribution Analysis: VEDA4 program (Warsaw, Poland, (2004). | [21] Palafox, M.A., Int. J. Quant. Chem., (2000) 77, 661–684. | | [22] Shettigar, V. Patil, P.S., Naveen, S., Dharmaprakash, S.M., Sridhar, M.A., Shashidhara Prasad, J., J. Cryst. Growth, (2007) 305, 218. | | [23] Gussoni, M., Castiglioni, C., J. Mol. Struct., (2003) 651, 151-158. | | [24] Palomar, J., De Paz, J.L, J. Catalan, Chem. Phys., (1999) 246, 167-208. | | [25] Rumi, M., Zerbi, G., J. Mol. Struct. (1999) 509, 11-28. | | [26] Meganathan, C., Sebastian, S., Kurt, M., Keun Woo Lee and N. Sundaraganesan J. Raman Spectrosc., (2010) 41, 1370–1378. | | [27] Poiyamozhi, A., Sundaraganesan, N., Karabacak, M., Tanrıverdi, O., Kurt, M., J. Mol. Struct., (2012) 1024, 1–12. | | [28] Balfour, J. W., Spectrochim. Acta., (1983) 39A, 795-800. | | [29] Lakshmaiah, B., Ramana Rao, G., J. Raman Spectrosc., (1989) 20, 439-448. | | [30] Lakshmaiah, B., Ramana Rao, G., Ind. J. Pure Appl. Phys., (1991) 29, 370-376. | | [31] Venkataram Reddy, B., Ramana Rao, G., Vib. Spectrosc., (1994) 6, 231-250 | | [32] Ashok Babu, V., Lakshmaiah, B., SreeRamulu, K., Ramana Rao, G., Ind. J. Pure Appl. Phys., (1987) 25, 58. | | [33] Sing, D.N., Yadav, R. A., Assian Chem. Lett., (1998) 2, 65-73. | [34] Prasad, R.L., Kushwaha, A., Suchita, M., Kumar, R.A., Yadav, Y., Spectrochim. Acta A (2008) 69, 304-311. | | [35] Sajan, D. Joe, I. H., and Jayakumar, J. Raman Spectrosc. (2006) 37, 508-519 | [36] Udhayakala, P., Jayanthi, A. Rajendiran, T.V., Gunasekaran, S., Archives of Applied Science Research., (2011) 3(4), 424-439. | [37] Varsanyi, G., Assignments for Vibrational Spectra of Seven Hundred Benzene Derivatives, Vol. 1–2, Academic Kiaclo, Budapet, (1973). | | [38] Pavia, D., Lampman, G.M. Kriz, G.S., Physics, third ed., in: J. Vondeling (Ed.), Introduction to Spectroscopy: A Guide for Student of Organic Chemistry, Vol. 579, Thomson Learning, (2001). | | [39] Jag, M., Organic Spectroscopy – Principles and Applications, second ed., Narosa Publishing House, New Delhi, (2001). | | [40] Krishnakumar, V., Xavier, R.J, Ind. J. Pure Appl. Phys., (2003) 41, 95–99. | | [41] Furic, K., Mohacek, V., Bonifacic, M., Stefanic, J. Mol. Struct., (1992) 267, 39–44. | [42] Zhang, H., Sun, Y., Chen, X., Yan, X., Sun, B., J. Cryst. Growth., (2011) 324, 196–200. | [43] The official web site of National Institute of Advanced Industrial Science and Technology (AIST), Research Information Database (RIO-DB). http://riodb.ibase.aist.go.jp/riohomee.html. | [44] Mani, P., Umamaheswari, H., Dominic Joshua, B., Sundaraganesan, N., J. Mol. Struct: THEOCHEM., (2008) 863, 44–49. | [45] Verdonck, L., Vander Kelen, G.P., Eeckhant, Z., Spectrochim. Acta 28A, (1972) 51. | [46] Hakan Arslan, Öztekin Algül, Int. J. Mol. Sci., (2007) 8, 760-776. | [47] Reed, A.E., Weinhold, F., J. Chem. Phys., (1985) 83, 1736-1740. | [48] Reed, A.E., Weinstock, R.B., Weinhold, F., J. Chem. Phys., (1985) 83, 735-746. | [49] Reed, A.E.., Weinhold, F., J. Chem. Phys., (1983) 78, 4066-4073. | [50] Foster, J.P., Wienhold, F., J. Am. Chem. Soc., (1980) 102, 7211–7218. | [51] Chocholousova, J., Vladimir Spirko, V., Hobza, P., J Chem. Phys., (2004) 6, 37–41. | [52] Handy, N., Maslen, P.E., Amos, R., Andrews, J.S., Murry, C.W., Laming, G.J., Chem. Phys. Lett., (1992) 197, 506–515. | [53] Anto, P.L., Anto R.J, Varghese H.T, Panicker, C.Y, Daizy Philipe, J. Raman Spectrosc. (2010) 41, 113–119. | [54] Sundius, T., J. Mol. Struct., (1990) 218, 321–326. | [55] Kleinman, D.A., Phys. Rev., (1962) 126, 1977. | [56] Alyar, H., Kantarci, Z., Bahat, M., Kasap, E., J. Mol. Struct., (2007) 834, 516–520. | [57] Castiglioni, C., Del Zoppo, M., Zuliani, P., Zerbi, G., Synth. Met., (1995) 74, 171-177. | [58] Zuliani, P., Del Zoppo. M., Castiglioni, C., Zerbi, G., Marder, S.R., Perry, J.W., Chem. Phys., (1995) 103, 9935-9940. | [59] Del Zoppo, M., Castiglioni, C., Zerbi, G., Non-Linear Opt., (1995) 9, 73. | [60] Del Zoppo, M., Castiglioni, C., Zuliani, P., Razelli, A., Zerbi, G., Blanchard-Desce, M., J. Appl. Polym. Sci., (1998) 70, 73. | [61] Ravikumar, C., Huber Joe, I., Jayakumar, V.S., Chem. Phys. Lett., (2008) 460, 552-558. | | [62] Kosar, B., Albayrak, C., Spectrochim. Acta Part A., (2011) 78, 160–167. | [63] Mulliken, R.S., J. Chem. Phys., (1955) 23, 1833–1840. | |